mater.scichina.com link.springer.com

Published online 17 June 2022 | https://doi.org/10.1007/s40843-022-2064-8
*Sci China Mater* 2022, 65(10): 2771–2778

# Molecule bridged graphene/Ag for highly conductive ink

Weixin Li[1,2,3], Jianmin Yan[1], Cong Wang[1], Ning Zhang[1], Tsz Hin Choy[1], Su Liu[5], Lei Zhao[2], Xiaoming Tao[4,5] and Yang Chai[1,3,4*]

**ABSTRACT** **Printing is a method of additive manufacturing that can reduce material costs and environmental contamination during the fabrication process. Ag ink is commonly used in printed electronics, such as interconnects, inductors, and antennas. However, the high cost of noble Ag restricts its massive applications. To reduce the cost of the state-of-the-art Ag ink and realize large-scale manufacturing, we develop a molecule-bridged graphene/Ag (MB-G/A) composite to produce highly conductive and cost-effective paper-based electronics. Graphene can be used to substitute part of Ag nanoparticles to reduce costs, form a conducive percolation network, and retain a reasonable level of conductivity. We adopt cysteamine as a molecular linker, because it anchors on the surface of graphene *via* the diazonium reaction. Additionally, the thiol functional group on the other end of cysteamine can bond to a Ag atom, forming a molecular bridge between graphene and Ag and promoting electron transport between Ag and graphene. As a result, the maximum conductivity of MB-G/A inks can reach 2.0 × $10^5$ S $m^{-1}$, enabling their successful application in various printable electronics. In addition, the optimum MB-G/A ink costs less than half as much as pure Ag inks, showing the great potential of MB-G/A ink in commercial electronic devices.**

**Keywords:** graphene, Ag, molecule modification, conductivity, flexible electronics

## INTRODUCTION

The continuous development of flexible electronics requires the direct fabrication of a large number of electronic devices and components on flexible substrates [1–3]. The conventional manufacturing process usually employs subtractive methods, which result in substantial material costs and environmental issues and are incompatible with the fabrication processes on flexible substrates [4]. The use of additive fabrication methods has become a dominant trend. Printing technology has been used for large-scale manufacturing of interconnects, inductors, and antennas [5–7]. The exploration of highly conductive inks with good uniformity, environmentally friendly fabrication techniques, and low cost is a crucial challenge for printed electronics. Generally, conductive inks are composed of conductive fillers and an organic matrix [8]. Conductive fillers, including metal nanoparticles, carbon nanomaterials, and conductive polymer, are a core element of electrically conductive inks.

Rational regulation of the composition, morphology, and distribution of the conductive fillers is essential to constructing an effective conductive path for achieving highly conductive inks. For example, Cui *et al.* [8] demonstrated the use of Ag micro-dendrites as fillers to form a conductive network with a low Ag filler loading. Considering the distribution of Ag fillers, Someya's group [9] described mixing micrometer-sized Ag flake with fluorine rubbers to *in-situ* form Ag nanoparticles. In addition, by designing core-shell structural particles (Ag@liquid metal micro/nanoparticles), real-time self-repair can be realized in the presence of external destruction [10]. Although Ag-based inks show excellent performance in various electronic devices, the high cost of Ag prevents their wide applications, particularly in certain scenarios with abundant materials consumption.

Alternatively, researchers have adopted some low-cost metals, e.g., copper [11], nickel [12], and aluminum [13], as conductive fillers to prepare high-performance inks. However, oxidation is an unavoidable issue [12,14]. To balance the cost and performance/stability, graphene stands out as a promising candidate for conductive fillers that possess desirable electrical properties and excellent stability [15–18]. Previously, our group demonstrated that the graphene coating on the Ag thin film exhibits high stability [19]. Researchers have devoted a lot of effort to acquiring graphene inks with superior conductivity [20]. For instance, Hu's group [21] reported high-quality and stable graphene flakes using non-toxic cyrene as the solvent, thus obtaining a highly concentrated graphene ink (7.13 × $10^4$ S $m^{-1}$). Ma's group [22] adopted graphene powders produced by jet cavitation and carbon black jointly as conductive fillers to obtain printed patterns with a conductivity of 2.1 × $10^4$ S $m^{-1}$. Chen's group [23] investigated the conductive inks made of single-layered graphene oxide (GO) and few-layered GO. However, the conductivity of carbon materials is still inferior to that of metal fillers. To enhance the electrical conductivity of inks, Baik's group [24] adopted hybrid fillers, such as Ag/carbon nanotube (CNT). However, the high junction resistance between the CNT and the agglomeration may lead to low conductivity. In addition, the π-π interaction between Ag and CNT is ineffective for electrical transport. Graphene-based hybrid fillers, usually pre-

[1] Department of Applied Physics, The Hong Kong Polytechnic University, Hong Kong 999077, China
[2] The State Key Laboratory of Refractories and Metallurgy, School of Materials and Metallurgy, Wuhan University of Science and Technology, Wuhan 430081, China
[3] The Hong Kong Polytechnic University Shenzhen Research Institute, Shenzhen 518057, China
[4] Research Center of Intelligent Wearable Systems, The Hong Kong Polytechnic University, Hong Kong 999077, China
[5] Institute of Textiles and Clothing, The Hong Kong Polytechnic University, Hong Kong 999077, China
* Corresponding author (email: y.chai@polyu.edu.hk)

  

pared by physical mixing, are used to increase the electroconductivity as well [25]. For instance, Sun's group [26] reported a printed GO/Ag composite film with good bend stability. Deng *et al.* [27] reported a Ag nanoparticle-decorated graphene conductive ink for flexible electronics. Although the unique two-dimensional (2D) basal plane structure and high specific surface area of graphene provide sufficient sites for loading Ag nanoparticles, the interaction between graphene and Ag is still ambiguous. The related study based on graphene/Ag hybrid inks rarely investigates the charge transport mechanism. Most of the work focuses on the dispersion issue of graphene in solvent to realize highly concentrated printable graphene ink, such as using solvent exchange, evaporation, and stabilizers [20,28,29]. Hence, revealing the mechanism of conductivity at a molecular scale is pivotal for realizing highly conductive graphene ink. The controllable modulation of conductive paths is a fundamental task for improving electrical performance of the printed flexible electronics.

In this study, we demonstrate a molecular bridge method for optimizing the charge transport process. The organic cysteamine molecule acts as a bridge between graphene and Ag nanoparticles, thus reinforcing the interaction between them at the molecular level. Cysteamine anchors on the surface of graphene *via* the diazonium reaction. At the same time, the thiol functional group on the other end of cysteamine can form a bond with a Ag atom, forming a molecular bridge between graphene and Ag. As a result, the conductive network is formed by graphene-Ag-graphene in the molecule-bridged graphene/Ag (MB-G/A), thus enhancing the charge transport between layered graphene flakes. The maximum conductivity patterns based on MB-G/A inks can reach $2.0 \times 10^5$ S m$^{-1}$ by adjusting the mass ratio of Ag and conductive fillers. As a result, the MB-G/A inks exhibit better electrical conductivity than those of graphene/Ag (without molecular bridge) inks and graphene inks. The successful application of MB-G/A inks to printed conductive circuits shows their future potential for various printable electronics.

## EXPERIMENTAL SECTION

### Preparation of the MB-G

Continuous ultrasonication was used to disperse 0.6 g of graphene (supplied by XFNANO) in 150 mL of deionized water (DI water) to form a homogeneous dispersion. Meanwhile, 1 mL of concentrated hydrochloric acid (HCl) solution was added to 5 mL of cysteamine (15 mmol) aqueous solution under ice bath condition, followed by 5 mL of sodium nitrite (15 mmol) aqueous solution. The as-prepared graphene dispersion solution was then added to the above solution and kept in an ice bath for 2 h. The resulting solution was then centrifuged and rinsed multiple times with DI water to obtain cysteamine-bridged graphene.

### Preparation of the MB-G/A

MB-G/A was synthesized *via* an *in-situ* reduction technique. Typically, the cysteamine-bridged graphene was dispersed in a mixed solution containing 25.0 mmol of glucose and 1.5 mmol of potassium sodium tartrate tetrahydrate ($V_{\text{DI water}}/V_{\text{ethonal}}$ = 9:1) and ultra-sonicated for 30 min. Meanwhile, a certain amount of silver nitrate (9.0, 13.0, and 17.0 mmol) was dissolved in DI water, accompanied by the addition of an ammonia solution to obtain silver ammonia solution. Then a sodium hydroxide aqueous solution (12.5 mmol) was added to stabilize the silver ammonia solution. Subsequently, the silver ammonia solution was dropped into the previously mixed solution (containing graphene and glucose) at the rate of 4 s/drop under constant magnetic stirring for 2 h. The obtained solution was centrifuged and washed with DI water several times and dried at 60°C under a vacuum to get MB-G/A. The MB-G/A obtained with different concentrations of silver nitrate possessed three kinds of mass ratios of Ag/C (1.4/1, 2.1/1, and 3/1), denoted as MB-G/A (1.4/1), MB-G/A (2.1/1), and MB-G/A (3/1), respectively. For comparison, graphene/Ag (G/A) (without cysteamine) was also prepared using the same process.

### Preparation of Ag nanoparticles

After dissolving 6.0 mmol of $AgNO_3$ in 50 mL of DI water, 0.5 mmol of sodium citrate dihydrate was added. Then, 50 mL of DI water containing 0.16 mol $FeSO_4{\cdot}7H_2O$ was continuously added to the above solution while stirring continuously until the color changed to grayish black. The products were centrifuged and rinsed numerous times with DI water to obtain Ag nanoparticles.

### Preparation of the conductive patterns

Art paper was employed as a flexible substrate for conductive patterns. First, the ethyl cellulose (2.5 wt%) was dissolved in the mixed organic solution ($V_{\text{ethanol}}$:$V_{\text{ethylene glycol}}$:$V_{\text{glycerol}}$ = 50:40:10). The above solution was then mixed with MB-G/A powder and ball milled for 12 h to produce MB-G/A ink. Graphene, G/A, and pure Ag conductive inks can be prepared by the same method but using graphene, G/A powder, and Ag powder instead of MB-G/A. The conductive patterns can be fabricated by direct printing with a designed mask on the art paper. After the printing, the patterns were heated at 150°C for 3 h to remove excess solvent and compression for further characterization.

### Computational details

To calculate the charge density difference between graphene and Ag, first-principle calculations were performed with the Vienna *ab initio* simulation packages (VASP) [30]. We adopted the Perdew-Burke-Ernzerhof (PBE) [31] parametrization of the generalized gradient approximation for the exchange-correlation energy. The force and the energy tolerance on each atom were less than 0.02 eV Å$^{-1}$ and $10^{-5}$ eV, respectively. The cut-off energy of the plane wave basis was 500 eV. A gamma centered $10 \times 10 \times 1$ Monkhorst-Pack *k*-point mesh was applied to the *k*-point samples in the Brillouin zone.

### Characterizations

The morphologies of MB-G/A powder and conductive patterns were characterized by field-emission scanning electron microscopy (SEM, TESCAN VEGA3). The composition and crystal structure were investigated by X-ray diffraction (XRD, Rigaku SmartLab 9kW). A WITEC confocal Raman system was adopted to record Raman spectra. Fourier transform infrared (FT-IR) spectra were performed with a Shimadzu Spectrum One FT-IR spectrophotometer. The X-ray photoelectron spectroscopy (XPS) measurements were collected by Thermo Fisher Nexsa. The thickness of the patterns was detected *via* the DektakXT Surface Profiler. The electrical property of the conductive patterns was measured using the four-probe resistivity/square resistance tester (CXT2665). Electrochemical impedance spec-

  

troscopy (EIS) measurements were performed on an electrochemical work station (Biologic vmp3) over a frequency range from 0.1 Hz to 100 kHz.

## RESULTS AND DISCUSSION

The schematic diagram of the fabrication process of MB-G/A is shown in Fig. 1a. As expected, diazonium salts ($HS–C_2H_4–NN^+Cl^-$) are *in-situ* reduced on the surface of graphene through the C–C bond, as displayed in equations (1) and (2) [32]. Meanwhile, the –SH groups of cysteamine can react with Ag nanoparticles to form Ag–S bonds because of their strong affinity for metal atoms [24,33]. The whole reaction for the synthesis of MB-G/A follows the equations (1–3) [32].

$$HS–CH_2–CH_2–NH_2 + NaNO_2 + 2HCl \rightarrow HS–CH_2–CH_2–N^+{\equiv}NCl^- + NaCl + 2H_2O, \quad (1)$$

$$HS–CH_2–CH_2–N^+{\equiv}NCl^- + \text{graphene} \rightarrow HS–CH_2–CH_2–\text{graphene} + N_2, \quad (2)$$

$$HS–CH_2–CH_2–\text{graphene} + Ag \rightarrow Ag–S–CH_2–CH_2–\text{graphene}. \quad (3)$$

In this way, we can obtain an MB-G/A composite. The morphologies of the MB-G/A with different mass ratios of Ag/C (1.4/1, 2.1/1, and 3/1) are shown in Fig. 1b–d. For comparison, the morphologies of the pristine graphene and G/A without molecular modification are shown in Fig. S1a, b. The average size of the graphene flake is approximately 5 μm, and its average thickness is approximately 5 nm (Fig. S1a). Many Ag nanoparticles are anchored on the surface of graphene, as shown in Fig. 1b. The majority of Ag nanoparticles are between 50 and 150 nm in size (Fig. S1d). The coverage of Ag nanoparticles on graphene improves, as the Ag/C mass ratio increases. Some of the Ag nanoparticles aggregate with each other due to the high concentration of $AgNO_3$. As for the G/A, severe aggregation appears on the surface of graphene. The size distribution of Ag nanoparticles is mainly in the range of 200–300 nm (Fig. S1c). The larger Ag nanoparticles and aggregate can be attributed to the lack of cysteamine molecules, thus leading to random dispersion of Ag nanoparticles on the graphene. The subsequently reduced Ag nanoparticles tend to grow on the pre-reduced Ag nanoparticles, resulting in worse uniformity and higher aggregation probability. As a result, the presence of cysteamine molecules can serve as anchor sites for Ag nanoparticles, thus promoting the dispersion of Ag nanoparticles homogenously with less aggregation. The uniform distribution of Ag nanoparticles is beneficial for better conductivity.

The XRD pattern (Fig. S2a) shows the crystal structures of the G/A and MB-G/A. The diffraction peaks match well with those of Ag (cubic, JCPDS 01-087-0717). The diffraction peaks at 38.1°, 44.3°, 64.4°, and 77.4° are indexed to the (111), (200), (220), and (311) planes of Ag crystals, respectively. The diffraction peaks at 26.5° and 54.6°, corresponding to the (002) and (004) planes, reflect a hexagonal graphite structure, which originate from the restacked graphene. The absence of other peaks confirms the successful fabrication of pure Ag crystalline on graphene without the introduction of impurities or oxidation in the MB-G/A.

To investigate the successful formation of MB-G/A, we characterized the sample using FT-IR spectroscopy (Fig. 2a). In both G/A and MB-G/A, a band at 1578 $cm^{-1}$ is associated with the C–C skeleton vibration of the carbon ring in graphene [34]. Two new peaks appear at around 2974 and 2886 $cm^{-1}$ after the modification by cysteamine molecules, which can be attributed to the symmetric and asymmetric vibrations of $CH_2$ [35]. In addition, the peak at 1046 $cm^{-1}$ arises due to the C–C stretching vibrations from cysteamine molecules [36]. The signals of $CH_2$ and C–C absorption peaks indicate the existence of cysteamine molecules. Additionally, the peak at 875 $cm^{-1}$, which is absent in G/A, belongs to the S-metal related bond, showing the presence of the Ag–S bond on the MB-G/A [37,38]. Furthermore, the FT-IR spectra of MB-G and pristine graphene were recorded to show the formation of the molecule bridge more clearly (Fig. S3a). The symmetric and asymmetric vibrations of $CH_2$ and

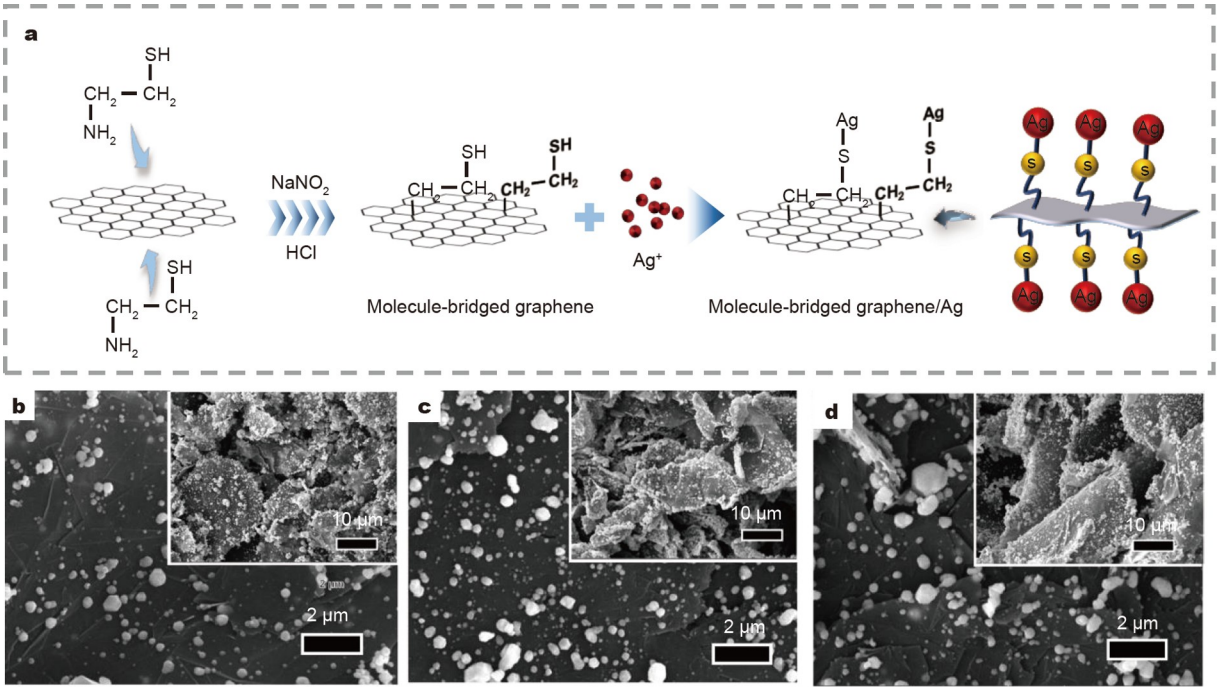


**Figure 1** (a) Schematic flow for fabricating MB-G/A. SEM images of (b) MB-G/A (1.4/1), (c) MB-G/A (2.1/1), and (d) MB-G/A (3/1).

  

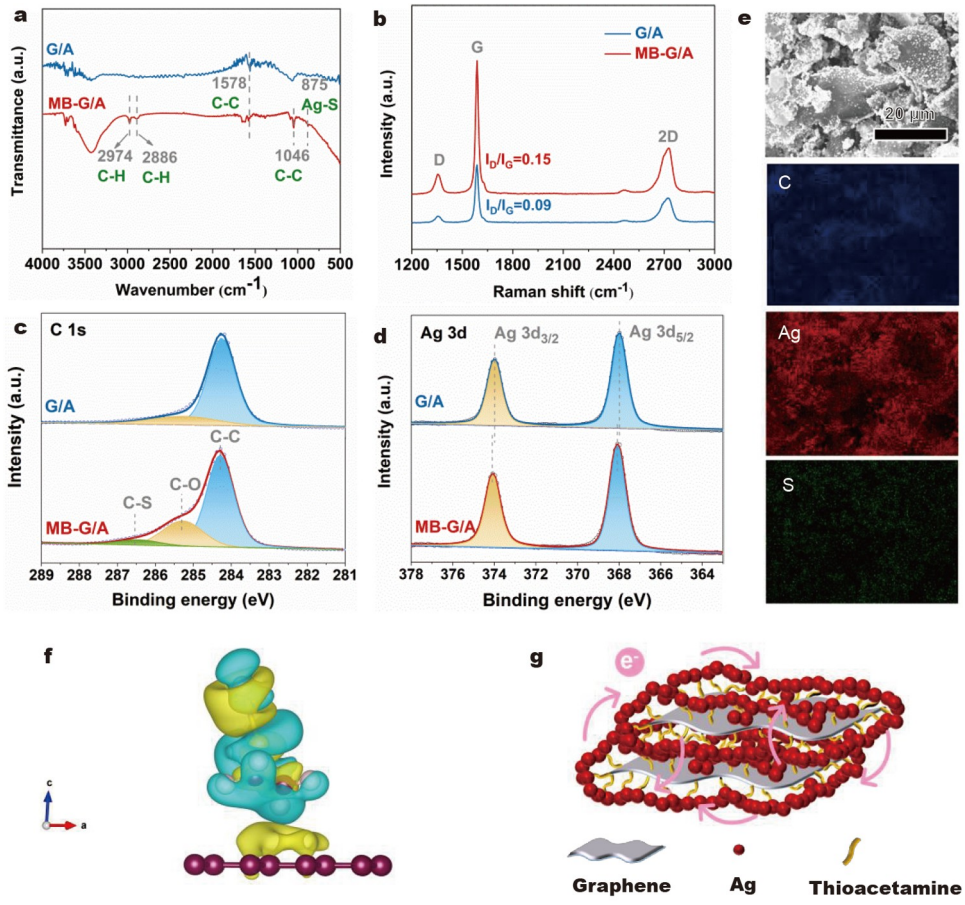


**Figure 2** (a) FT-IR spectra, (b) Raman spectra, (c) C 1s XPS spectra, and (d) Ag 3d XPS spectra of G/A and MB-A/G, respectively, (e) EDX mapping images of MB-G/A. (f) Charge density difference of MB-G/A. The yellow region implies electron gain, while the blue region shows electron depletion. (g) Conductive network diagram of MB-G/A.

the C–C stretching vibrations from cysteamine molecules can be detected in MB-G as well, which are absent in the pristine graphene. Additionally, these results show that cysteamine molecules are covalently bridged on the surface of graphene and Ag nanoparticles *via* C–C bonds and thiol groups, respectively.

Raman spectroscopy was used to further investigate the structure of MB-G/A. As shown in Fig. 2b, the peak at 1354 $cm^{-1}$ corresponds to the D band, which is associated with graphene's disorder and defects caused by the $sp^3$ hybridized carbon. The characteristic peak of the G band at 1587 $cm^{-1}$ is caused by the $E_{2g}$ phonon of $sp^2$-bonded carbon atoms [39]. The intensity ratio of D and G bands ($I_D/I_G$) of MB-G/A is approximately 0.15, which is greater than that of G/A (0.09). Additionally, the $I_D/I_G$ value of MB-G (0.13) is greater than that of the pristine graphene (0.09) (Fig. S3b). Apart from the increased $I_D/I_G$ value, the G band and 2D bands of MB-G show a positive shift (about 8 $cm^{-1}$) compared with pristine graphene due to the strain caused by the grafted molecule [40]. The increased $I_D/I_G$ value combined with the shift of Raman peaks of cysteamine molecules indicates a partially changed $sp^2$ structure and structural disorder in the lattice of pristine graphene due to the covalent modification of cysteamine molecules on graphene.

We investigated the chemical states of G/A and MB-G/A by XPS. The deconvoluted C 1s spectrum of MB-G/A can be resolved into three peaks at 284.3, 285.3, and 286.5 eV, as shown in Fig. 2c. The primary peak at 284.3 eV belongs to the $sp^2$ hybridized C–C bond in a graphitic lattice [41]. The peak at 285.3 eV is associated with a C–O bond, which originates from the air oxidation and liquid reduction processes, resulting in the oxidation of C atoms next to the bonding site of cysteamine molecules [32]. The peak at 286.5 eV shows the presence of C–S species. C 1s spectra for MB-G and pristine graphene are similar (Fig. S3c), showing that the cysteamine molecules have been successfully bridged on the graphene [42,43]. In addition, the Ag 3d peaks in G/A from 367.9 eV ($3d_{5/2}$) and 373.9 eV ($3d_{3/2}$) shift to higher binding energies of 368.1 and 374.1 eV in MB-G/A (Fig. 2d) [33], implying the formation of Ag–S bonds, which is consistent with the results of FT-IR. The peaks of S 2p at 163.1 and 168.4 eV can be detected in MB-G/A, as shown in survey XPS spectra (Fig. S2), showing the presence of C–S and Ag–S species on the surface of graphene [44–46]. In addition, energy dispersive X-ray spectroscopy (EDX) mapping of MB-G/A was recorded to clarify the element distribution, which showed Ag, C, and S (Fig. 2e).

Density functional theory (DFT) calculation of the charge density distribution was performed to show the charge transfer between Ag and graphene, in which the blue and yellow colors represent the electron depletion and accumulation, respectively. As shown in Fig. 2f, the charge accumulation appears around the C atom in graphene, and the C atoms in cysteamine show an electron depletion phenomenon, demonstrating the establishment of an electronic channel in the interface of graphene and

  

cysteamine molecules. The covalent bonds between graphene and cysteamine are stronger interactions than those of electrostatic interactions, hydrogen bonds, and van der Waals forces, thus indicating efficient interfacial interaction between graphene and cysteamine [47,48]. The electrons can be transferred from cysteamine molecules to graphene. According to the Ag–S bond theory, the 5s-orbital lone electron of Ag atoms can easily migrate to the electron hybrid orbitals of S atoms and form a strong Ag–S bond [49]. Thus, the overlapping of electron clouds between the S atom in cysteamine molecules and the Ag atom shows that charges from the Ag atoms are transferred to the cysteamine molecules, which is consistent with the XPS results. As a result, the DFT results verify that the molecule at the interface between graphene and Ag nanoparticle accelerates electron transfer kinetics. The conductive network of MB-G/A is schematically shown in Fig. 2g. In MB-G/A, cysteamine molecules, which serve as charge transport channels, promote the charge transfer process in both vertical and horizontal directions. However, charge transfer in the vertical direction faces a high barrier in G/A due to the lack of an effective transport channel. As a result, MB-G/A will show superior electroconductivity.

The prepared MB-G/A powder was used as a conductive filler and homogenously dispersed in organic solvent to obtain MB-G/A ink for further electrical conductivity characterization. The mass ratio of conductive filler was adjusted to evaluate the effects of the concentration of conductive filler on the electrical conductivity of the printed patterns. For reference, the pristine graphene and G/A were adopted as conductive fillers by the same fabrication process. Due to the high specific surface area of graphene, the maximum mass ratio of graphene ink can only reach 16%. The graphene ink will become sticky and hard to print due to the low fluidity and high density caused by the further increase in graphene mass ratio. The electrical conductivity of graphene ink increases along with the mass ratio, with the highest conductivity reaching $3.3 \times 10^4$ S m$^{-1}$ (Fig. S4). By comparison, 16, 20, 24, 28, and 32 wt% of MB-G/A were used as alternatives to pristine graphene. As expected, the conductivity of patterns shows dramatic improvement with the increase of Ag loading in graphene nanosheets (Fig. 3a–c). As shown in Fig. 3a, 16 wt% MB-G/A ink shows a conductivity of $4.1 \times 10^4$ S m$^{-1}$, and the conductivity of 32 wt% MB-G/A ink exceeds $1.0 \times 10^5$ S m$^{-1}$, demonstrating the increased trend of conductivity along with the mass ratio of conductive fillers. With the increase of conductive fillers, the amount of Ag loading will be increased as well. Additionally, the increased concentration of conductive fillers facilitates the contact between conductive fillers, thus forming more conductive paths [22,50].

The mass ratio of Ag/C in MB-G/A was adjusted by controlling the molar ratio of silver nitrate to demonstrate the impacts of Ag nanoparticles. As shown in Fig. 3a–c, we prepared three different mass ratios of Ag/C (1.4/1, 2.1/1, and 3/1), all of which show similar behavior when the mass ratio of conductive fillers is changed. The 32 wt% MB-G/A (2.1/1) achieves a conductivity of $1.7 \times 10^5$ S m$^{-1}$, which is about 1.7 times that of the 32 wt% MB-G/A (1.4/1). Further increasing the Ag/C mass ratio results in a relatively small enhancement of conductivity ($2.0 \times 10^5$ S m$^{-1}$) for the 32 wt% MB-G/A (3/1). According to the results of SEM morphology characterization (Fig. 1), Ag nanoparticles are primarily distributed on the surface of graphene flakes, with a small amount of Ag nanoparticles located on the edge of graphene flakes for MB-G/A (1.4/1). However, when the concentration of silver nitrate increases, Ag nanoparticles anchor on not only the surface but also the edges of graphene flakes in the MB-G/A (2.1/1). The well-covered edges of graphene flakes by Ag nanoparticles promote the interaction of graphene flakes, resulting in the formation of more graphene-Ag-graphene conductive paths and improved electrical conductivity. After increasing the silver nitrate concentration (MB-G/A (3/1)), the established conductive network shows little change, with only more Ag nanoparticles agglomerating on the surface and edges of graphene flakes. On the one hand, increasing the concentration of Ag nanoparticles improves electrical conductivity due to the superior electrical property of Ag. On the other hand, the agglomeration of Ag nanoparticles can increase the gap between graphene flakes, resulting in a discontinuous conductive network. SEM images of patterns printed with three different types of ink (Fig. S4b–d) show that the distribution of Ag nanoparticles continuously increases with the molar ratio of silver nitrate. The agglomeration of Ag nanoparticles is visible in the MB-G/A (3/1) pattern. Consequently, MB-G/A (2.1/1) ink shows a significant increase in conductivity while the enhancement of MB-G/A (3/1) ink is plain. To demonstrate the effect of cysteamine molecules on electrical conductivity, a series of G/A (3/1) conductive filler-based inks were prepared with the electrical conductivity, and the results are shown in Fig. S4f. The conductivity of patterns printed with 32% G/A (3/1) ink is $1.5 \times 10^5$ S m$^{-1}$, which is less than that of their counterparts (32% MB-G/A (3/1)). The SEM images (Fig. 1d and Fig. S1b) show that the morphology differences between MB-G/A (3/1) and G/A (3/1) are primarily due to the size distribution of Ag nanoparticles. Hence, the inferior electrical conductivity of G/A (3/1) can be attributed to the increased aggregation of Ag nanoparticles and the absence of a charge transport channel, as corroborated by the DFT results. To explore the potential application of the MB-G/A ink, the material cost is determined using the commercial price. Pure Ag inks (mass ratio of Ag nanoparticles is 60 wt%) are prepared for comparison. The conductivity of pure Ag inks is over 12 times that of the optimum MB-G/A ink (Fig. 3d). However, the cost of the optimum MB-G/A ink is less than half as much as the pure Ag inks (Fig. S4g). As a result, the MB-G/A ink possesses great potential in commercial electronic devices.

The MB-G/A ink was printed as the electrodes to evaluate their electrical performance in the conductivity experiment. The electrode patterns include two 1 cm × 1 cm squares separated by a 2-mm gap. The EIS measurements were performed using a phosphate-buffered saline (PBS; pH 7.4) buffer solution as the electrolyte [51]. The EIS spectra are shown in Fig. 3e, with an inset showing the change of impedance along with frequency. At low frequencies, the impedance is associated with the ion diffusion resistance. At high frequencies, the impedance is related to both charge transport and electrical resistance [52–54]. As expected, MB-G/A (3/1) has the lowest charge transport resistance in the high-frequency range. And the inset of Fig. 3e shows that the electrode patterns based on MB-G/A (3/1) have the lowest electrical impedance values across the whole frequency range, showing the lowest resistance, which is consistent with the conductivity results previously stated. Bending tests were performed to determine the flexibility of MB-G/A printed on art paper. The change in electrical resistance corresponding to the original resistance ($\Delta R/R_0$) of the printed pattern during 100

  

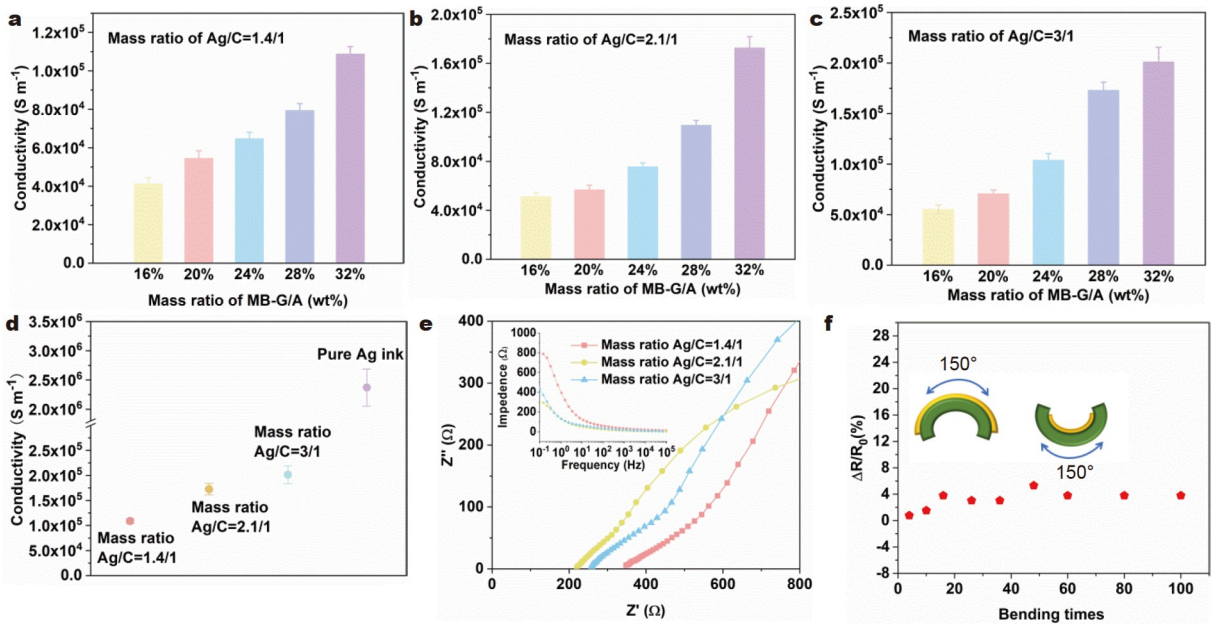


**Figure 3** Conductivity of patterns based on (a) MB-G/A (1.4/1) ink, (b) MB-G/A (2.1/1) ink, and (c) MB-G/A (3/1) ink, (d) conductivity comparison of patterns based on different inks, (e) EIS spectra of different printed electrodes in the frequency range from 0.1 Hz to 10 kHz, and (f) bending test of patterns based on MB-G/A (3/1) ink.

bending cycles is shown in Fig. 3f. It is acceptable for the electrical resistance of the printed pattern to increase slightly as the number of bending cycles increases, as this can be caused by bending cracks. Although graphene is intrinsically flexible, numerous bends in both directions will result in cracks at the interface, such as graphene or Ag nanoparticles. A mismatch in the elastic constant between the substrate (art paper) and the patterns can also result in cracks after the bending. However, the variation in resistance is less than 6%, showing its prospective application in flexible devices.

Furthermore, we printed the MB-G/A ink on the art paper to show how it might be applied in flexible electronics. Two conductive lines were printed onto the art paper with MB-G/A ink to assemble a light-emitting diode (LED). As shown in Fig. 4a, LEDs on the printed lines are lighting. The treatment of 180° bending and twisting of two circles of the pattern will not affect the light illuminating of the LED, showing the promising potential application of more complicated flexible conductive patterns. When immersing the assembled LED on two conductive lines printed on the art paper in water, the LED can maintain illumination, as shown in Fig. 4b. The wet-dry cycle test was conducted to illustrate the stability of the printed patterns when exposed to water. Specifically, the printed patterns on art papers were immersed in water for 5 s and then dried on the hot plate at 80°C for one cycle. The change of electrical resistance relative to the original resistance ($\Delta R/R_0$) of the printed pattern after ten cycles is less than 20%, demonstrating the stability of the printed patterns.

In addition, we fabricated inductors by printing rectangular spiral inductors on the art paper with line widths and spacing of 3 and 3 mm. An LED was connected to the printed rectangular spiral inductors. The power source was connected with a small motor and a copper coil (Fig. 4c). When we place the printed rectangular spiral inductors on top of the copper coil, the LED lights up, showing that the printed rectangular spiral pattern can

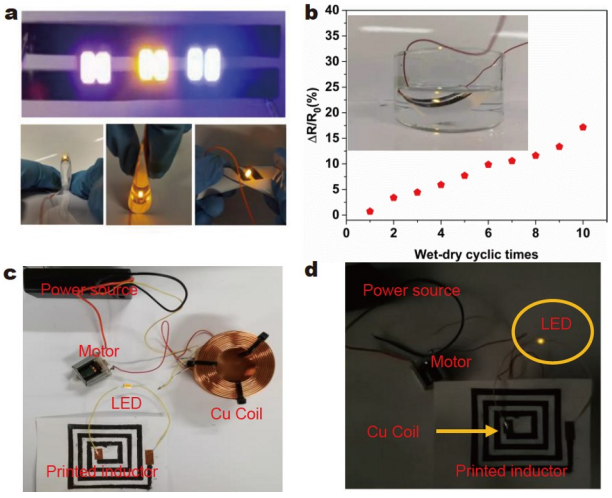


**Figure 4** (a) Illumination of an LED with flexible MB-G/A ink printed lines on the art paper. (b) Wet stability of patterns based on the MB-G/A ink (inset is the printed pattern with an LED in water). Printed inductance test: (c) printed rectangular spiral inductors put aside the copper coil, and (d) printed rectangular spiral inductors put on the copper coil.

work as inductors for near-field power transmission, as shown in Fig. 4d (video S1). These results show that the MB-G/A ink can meet the requirements of flexible and printable electronics applications.

## CONCLUSIONS

In summary, we demonstrate a molecular bridge method to prepare a Ag-anchored graphene ink. Cysteamine anchors on the surface of graphene *via* the diazonium reaction, while the thiol functional group on the other end of cysteamine can bond with a Ag atom, resulting in an effective graphene-Ag-graphene conductive channel in MB-G/A. The spectroscopic character-

ization results demonstrate the presence of cysteamine molecules in MB-G/A. The conductivity performance of patterns based on the MB-G/A inks is $2.0 \times 10^5$ S m$^{-1}$, which is higher than the patterns made with the G/A inks. The DFT results combined with electrical characterization show the effective electron transport *via* the molecule bridge, accompanied by the promoted charge transport process between layered graphene flakes. Although the conductivity of the pure Ag inks is almost 12 times the conductivity of the optimum MB-G/A ink, the optimum MB-G/A ink costs less than half as much as pure Ag inks. The successful application of the acquired MB-G/A inks in flexible electron circuits and inductors shows that the MB-G/A inks can meet the requirements of low-temperature, flexible, and printable electronics.

**Received 5 January 2022; accepted 6 April 2022; published online 17 June 2022**


1 Hsieh TL, Li CC, Lin PC, *et al.* Encapsulating well-dispersed carbon nanoparticles for applications in the autonomous restoration of electronic circuits. ACS Appl Mater Interfaces, 2020, 12: 38690–38699
2 Khan Y, Thielens A, Muin S, *et al.* A new frontier of printed electronics: Flexible hybrid electronics. Adv Mater, 2020, 32: 1905279
3 Li W, Zhang H, Kagita S, *et al.* All screen-printed, polymer-nanowire based foldable electronics for mm-wave applications. Adv Mater Technologies, 2021, 6: 2100525
4 Gysling HJ. Nanoinks in inkjet metallization—Evolution of simple additive-type metal patterning. Curr Opin Colloid Interface Sci, 2014, 19: 155–162
5 Hyun WJ, Secor EB, Hersam MC, *et al.* High-resolution patterning of graphene by screen printing with a silicon stencil for highly flexible printed electronics. Adv Mater, 2015, 27: 109–115
6 Hyun WJ, Park OO, Chin BD. Foldable graphene electronic circuits based on paper substrates. Adv Mater, 2013, 25: 4729–4734
7 Ibanez-Labiano I, Ergoktas MS, Kocabas C, *et al.* Graphene-based soft wearable antennas. Appl Mater Today, 2020, 20: 100727
8 Yang C, Cui X, Zhang Z, *et al.* Fractal dendrite-based electrically conductive composites for laser-scribed flexible circuits. Nat Commun, 2015, 6: 8150
9 Matsuhisa N, Inoue D, Zalar P, *et al.* Printable elastic conductors by *in situ* formation of silver nanoparticles from silver flakes. Nat Mater, 2017, 16: 834–840
10 Zheng R, Peng Z, Fu Y, *et al.* A novel conductive core-shell particle based on liquid metal for fabricating real-time self-repairing flexible circuits. Adv Funct Mater, 2020, 30: 1910524
11 Stewart IE, Rathmell AR, Yan L, *et al.* Solution-processed copper-nickel nanowire anodes for organic solar cells. Nanoscale, 2014, 6: 5980–5988
12 Mohammadi MM, Gunturi SS, Shao S, *et al.* Flame-synthesized nickel-silver nanoparticle inks provide high conductivity without sintering. Chem Eng J, 2019, 372: 648–655
13 Kiełbasiński K, Krzemiński J, Młożniak A, *et al.* New technology of silvering aluminium busbar joints with the use of printable paste containing nano-size Ag particles. J Mater Sci-Mater Electron, 2015, 26: 1832–1837
14 Kamyshny A, Magdassi S. Conductive nanomaterials for printed electronics. Small, 2014, 10: 3515–3535
15 Zhao Y, Xie Y, Liu Z, *et al.* Two-dimensional material membranes: An emerging platform for controllable mass transport applications. Small, 2014, 10: 4521–4542
16 Wang M, Cai L, Wang Y, *et al.* Graphene-draped semiconductors for enhanced photocorrosion resistance and photocatalytic properties. J Am Chem Soc, 2017, 139: 4144–4151
17 Zhao Y, Liu Z, Sun T, *et al.* Mass transport mechanism of Cu species at the metal/dielectric interfaces with a graphene barrier. ACS Nano, 2014, 8: 12601–12611
18 Yang X, Li XM, Kong QQ, *et al.* One-pot ball-milling preparation of graphene/carbon black aqueous inks for highly conductive and flexible printed electronics. Sci China Mater, 2020, 63: 392–402
19 Zhao Y, Xie Y, Hui YY, *et al.* Highly impermeable and transparent graphene as an ultra-thin protection barrier for Ag thin films. J Mater Chem C, 2013, 1: 4956–4961
20 Karagiannidis PG, Hodge SA, Lombardi L, *et al.* Microfluidization of graphite and formulation of graphene-based conductive inks. ACS Nano, 2017, 11: 2742–2755
21 Pan K, Fan Y, Leng T, *et al.* Sustainable production of highly conductive multilayer graphene ink for wireless connectivity and IoT applications. Nat Commun, 2018, 9: 5197
22 Liu L, Shen Z, Zhang X, *et al.* Highly conductive graphene/carbon black screen printing inks for flexible electronics. J Colloid Interface Sci, 2021, 582: 12–21
23 Huang L, Huang Y, Liang J, *et al.* Graphene-based conducting inks for direct inkjet printing of flexible conductive patterns and their applications in electric circuits and chemical sensors. Nano Res, 2011, 4: 675–684
24 Chun KY, Oh Y, Rho J, *et al.* Highly conductive, printable and stretchable composite films of carbon nanotubes and silver. Nat Nanotech, 2010, 5: 853–857
25 Jia H, Yi ZL, Huang XH, *et al.* A one-step graphene induction strategy enables *in-situ* controllable growth of silver nanowires for electromagnetic interference shielding. Carbon, 2021, 183: 809–819
26 Cui B, Chu F, Li H, *et al.* Inkjet printing porous graphene/silver flexible electrode with enhanced electrochemical performance based on vapor phase reduction. J Mater Sci-Mater Electron, 2020, 31: 10795–10802
27 Deng D, Feng S, Shi M, *et al. In situ* preparation of silver nanoparticles decorated graphene conductive ink for inkjet printing. J Mater Sci-Mater Electron, 2017, 28: 15411–15417
28 Arapov K, Rubingh E, Abbel R, *et al.* Conductive screen printing inks by gelation of graphene dispersions. Adv Funct Mater, 2016, 26: 586–593
29 Tkachev S, Monteiro M, Santos J, *et al.* Environmentally friendly graphene inks for touch screen sensors. Adv Funct Mater, 2021, 31: 2103287
30 Kresse G, Furthmüller J. Efficient iterative schemes for *ab initio* total-energy calculations using a plane-wave basis set. Phys Rev B, 1996, 54: 11169–11186
31 Perdew JP, Burke K, Ernzerhof M. Generalized gradient approximation made simple. Phys Rev Lett, 1996, 77: 3865–3868
32 Hossain MZ, Shimizu N. *In situ* functionalization of graphene with reactive end group through amine diazotization. J Phys Chem C, 2017, 121: 25223–25228
33 Liu GS, Xu Y, Kong Y, *et al.* Comprehensive stability improvement of silver nanowire networks *via* self-assembled mercapto inhibitors. ACS Appl Mater Interfaces, 2018, 10: 37699–37708
34 Lin WD, Chang HM, Wu RJ. Applied novel sensing material graphene/polypyrrole for humidity sensor. Sens Actuat B-Chem, 2013, 181: 326–331
35 Hou L, Hu Z, Wu H, *et al.* 2-Amino-3-chloro-1,4-naphthoquinone-covalent modification of graphene nanosheets for efficient electrochemical energy storage. Dalton Trans, 2019, 48: 9234–9242
36 Robidillo CJT, Aghajamali M, Faramus A, *et al.* Interfacing enzymes with silicon nanocrystals through the thiol-ene reaction. Nanoscale, 2018, 10: 18706–18719
37 Yuan S, Wang Y, Zhang Y, *et al.* CdS nanospheres hybridized with graphitic $C_3N_4$ for effective photocatalytic hydrogen generation under visible light irradiation. Appl Organometal Chem, 2019, 33: e4671
38 Kadian S, Manik G, Das N, *et al.* Synthesis, characterization and investigation of synergistic antibacterial activity and cell viability of silver-sulfur doped graphene quantum dot (Ag@S-GQDs) nanocomposites. J Mater Chem B, 2020, 8: 3028–3037
39 Jia H, Kong QQ, Yang X, *et al.* Dual-functional graphene/carbon nanotubes thick film: Bidirectional thermal dissipation and electromagnetic shielding. Carbon, 2021, 171: 329–340
40 He S, Xie W, Zhang Y, *et al.* Investigation of substrate swell-induced defect formation in suspended graphene upon helium ion implantation. J Phys Chem C, 2021, 125: 16166–16174
41 Ashok A, Kumar A, Ponraj J, *et al.* Synthesis and growth mechanism of


  

bamboo like N-doped CNT/graphene nanostructure incorporated with hybrid metal nanoparticles for overall water splitting. Carbon, 2020, 170: 452–463
42 Zhai C, Sun M, Zhu M, *et al.* A new method to synthesize sulfur-doped graphene as effective metal-free electrocatalyst for oxygen reduction reaction. Appl Surf Sci, 2017, 407: 503–508
43 Gu W, Sevilla M, Magasinski A, *et al.* Sulfur-containing activated carbons with greatly reduced content of bottle neck pores for double-layer capacitors: A case study for pseudocapacitance detection. Energy Environ Sci, 2013, 6: 2465
44 Liu P, Wang H, Yan T, *et al.* Grafting sulfonic and amine functional groups on 3D graphene for improved capacitive deionization. J Mater Chem A, 2016, 4: 5303–5313
45 Dong M, Wang Z, Li X, *et al.* Vital effect of sufficient vulcanization on the properties of Ni-Co-S/graphene composites for supercapacitor. Chem Eng Sci, 2020, 221: 115709
46 Luo Y, Yuan D, Balogun MS, *et al.* Dual doping strategy enhanced the lithium storage properties of graphene oxide binary composites. J Mater Chem A, 2016, 4: 13431–13438
47 Silvera Batista CA, Larson RG, Kotov NA. Nonadditivity of nanoparticle interactions. Science, 2015, 350: 1242477
48 Pan XF, Gao HL, Su Y, *et al.* Strong and stiff Ag nanowire-chitosan composite films reinforced by Ag–S covalent bonds. Nano Res, 2018, 11: 410–419
49 Yu H, Fang D, Dirican M, *et al.* Binding conductive ink initiatively and strongly: Transparent and thermally stable cellulose nanopaper as a promising substrate for flexible electronics. ACS Appl Mater Interfaces, 2019, 11: 20281–20290
50 Saborio MG, Cai S, Tang J, *et al.* Liquid metal droplet and graphene co-fillers for electrically conductive flexible composites. Small, 2020, 16: 1903753
51 Fernandes IJ, Aroche AF, Schuck A, *et al.* Silver nanoparticle conductive inks: Synthesis, characterization, and fabrication of inkjet-printed flexible electrodes. Sci Rep, 2020, 10: 8878
52 Li X, Qin Z, Fu H, *et al.* Enhancing the performance of paper-based electrochemical impedance spectroscopy nanobiosensors: An experimental approach. Biosens Bioelectron, 2021, 177: 112672
53 Tang Y, Zhang Y, Rui X, *et al.* Conductive inks based on a lithium titanate nanotube gel for high-rate lithium-ion batteries with customized configuration. Adv Mater, 2016, 28: 1567–1576
54 Hondred JA, Stromberg LR, Mosher CL, *et al.* High-resolution graphene films for electrochemical sensing *via* inkjet maskless lithography. ACS Nano, 2017, 11: 9836–9845

**Acknowledgements** This work was financially supported by Hong Kong Scholars Program (XJ2019025), The Hong Kong Polytechnic University (CD42), and Shenzhen Science and Technology Innovation Commission (JCYJ20180507183424383).

**Author contributions** Li W performed most of the experiments and wrote the original manuscript. Yan J participated in some experiments. Wang C conducted the simulations. Zhang N and Choy TH conducted some investigations. Liu S and Zhao L offered some methodology. Tao X reviewed and edited the manuscript. Chai Y planned and supervised the research.

**Conflict of interest** The authors declare that they have no conflict of interest.

**Supplementary information** Supporting data are available in the online version of the paper.

**Weixin Li** received her bachelor degree from Wuhan University of Technology in 2011. She earned her PhD degree from Huazhong University of Science and Technology in 2016. She is now an associate professor at Wuhan University of Science and Technology. Her research interests include the design and synthesis of advanced energy conversion systems, such as water splitting devices and solar cells.

**Yang Chai** is an assistant dean of the Faculty of Applied Science and Textile of The Hong Kong Polytechnic University, *vice* president of Physical Society of Hong Kong, a member of The Hong Kong Young Academy of Sciences, an IEEE Distinguished Lecturer since 2016, and was the chair of IEEE ED/SSC Hong Kong Chapter (2017–2019). His current research interest mainly focuses on emerging electronic devices.

## 分子桥连石墨烯/银用于高性能导电浆料

李薇馨[1,2,3], 晏建民[1], 王聪[1], 张宁[1], 蔡子轩[1], 刘苏[5], 赵雷[2], 陶肖明[4,5], 柴扬[1,3,4*]

**摘要** 印刷作为一种增材制备技术可以降低制备过程中的材料成本并减少对环境的污染. 银导电浆料常用于各种电子印刷器件, 如互联网、电感、天线等领域. 然而贵金属银的高成本限制了其大规模应用. 为了降低目前银导电浆料的成本, 本文提出了一种分子桥连的石墨烯/银(MB-G/A)导电浆料, 并应用于高导电性、低成本的纸基电子器件. 石墨烯可以取代部分银纳米颗粒, 降低成本的同时形成合适的导电网络, 从而保证了良好的导电性能. 采用巯基乙胺作为分子桥连剂, 其一端通过叠氮反应锚定在石墨烯表面, 另一端通过巯基官能团与银原子成键, 实现石墨烯和银之间分子尺度的桥连, 从而促进石墨烯/银界面的电荷传输. 结果表明所制备的MB-G/A导电浆料的最大电导率可达2.0 × $10^5$ S $m^{-1}$, 且可成功应用于各种电子器件中. 此外, 最优的MB-G/A导电浆料的成本与纯银导电浆料相比减少了至少一半. 该MB-G/A导电浆料在商业化电子器件领域具有良好的应用前景.

  